Electronic Supplementary information

Carbon-coated shuttle like $Fe_2O_3/Fe_{1-x}S$ heterostructure derived from metal-organic frameworks with high pseudocapacitance for ultrafast lithium storage

Guang Zhu[a], Xiaojie zhang [b,c], Yanjiang Lia, guangzhen Zhao[a], Haifeng Xu[a*], Zhong Jin[d]*

a Key Laboratory of Spin Electron and Nanomaterials of Anhui Higher Education Institutes, Suzhou University, Suzhou 234000, P. R. China

b National & Local Joint Engineering Research Center for Mineral Salt Deep Utilization, Key Laboratory for Palygorskite Science and Applied Technology of Jiangsu Province, Huaiyin Institute of Technology, Huaian 223003, China

c School of Electrical and Power Engineering, China University of Mining and Technology, Xuzhou, 221116, China

d Key Laboratory of Mesoscopic Chemistry of MOE, Jiangsu Key Laboratory of Advanced Organic Materials, School of Chemistry and Chemical Engineering, Nanjing University, Nanjing 210023, China

[*] Corresponding author. Tel.: +86 557 2871680; *E-mail address: guangzhu@ahsztc.edu.cn; Xuhaifeng@ahszu.edu.cn*

Materials **Characterization:** The morphologies, structures and phases of the as-prepared samples were identified via field emission scanning electron microscopy (SEM, S-4800, Hitachi) with energy dispersive X-ray spectroscopy (EDS), transmission electron microscopy (TEM, JEOL-2010) and X-ray diffraction (XRD, Smart lab, Rigaku) with Cu-Kα radiation (λ=1.5418 Å). The specific surface areas of the samples were calculated from the nitrogen adsorption/desorption isotherms (Micromeritics, ASAP 2020 at 77 K) based the Brunauer-Emmett-Teller (BET) method and the corresponding pore size distribution was deduced from the adsorption segments using Barret-Joyner-Halenda (BJH) method. Raman spectra were recorded on a Raman spectrometer (Horiba, Scientific) with an argon-ion laser excitation wavelength of 532 nm.

Electrochemical test: The electrochemical characterizations of the as-prepared samples were tested by half-Li cells assembled in 2032-type coin cells. The electrodes were fabricated by grinding Fe_2O_3@C or $Fe_2O_3/Fe_{1-x}S$@C as active material, Super P as conducting agent and carboxyl methyl cellulose dissolved in deionized water as binder in a mass ratio of 7:2:1 to form a homogenously slurry. Then the slurry was doctor-bladed onto a copper foil used as current collector by an automatic thick film coater, and then dried in a vacuum oven at 120 °C for 24 h to remove excess water completely. The cells were assembled in a glove box (MB-10-compact, MBRAUN) under Ar atmosphere where the contents of oxygen and water were less than 0.5 ppm. Pure metal lithium foil was used as both reference and counter electrodes and whatman glass fiber membrane was used as separator. The electrolyte used in the coin

cells was composed of 1 mol L^{-1} $LiPF_6$ dissolved in ethylene carbonate and propylene carbonate (1:1, w/w). Cycling tests were carried out at a current density of 0.1 A g^{-1} unless otherwise specified by a LAND2001A battery test system in a voltage range of 0.005-3.0 V (vs. Li^+/Li). The specific capacity was calculated based on the total mass of the active materials. The mass loading of Fe_2O_3@C or $Fe_2O_3/Fe_{1-x}S$@C is approximately 1.5 mg cm^{-2}. The cyclic voltammetry (CV) was recorded on an electrochemical workstation (Autolab PGSTA302N) between 0.005 and 3.0 V at various scan rates from 0.2 to 1.4 mV s^{-1}. The electrochemical impedance spectroscopy (EIS) measurement was conducted on the same electrochemical workstation after 100 charge/discharge cycles in a frequency range of 0.1 Hz to 100 kHz, where the applied bias voltage and ac amplitude were set at the open circuit voltage of the cells and 5 mV, respectively.

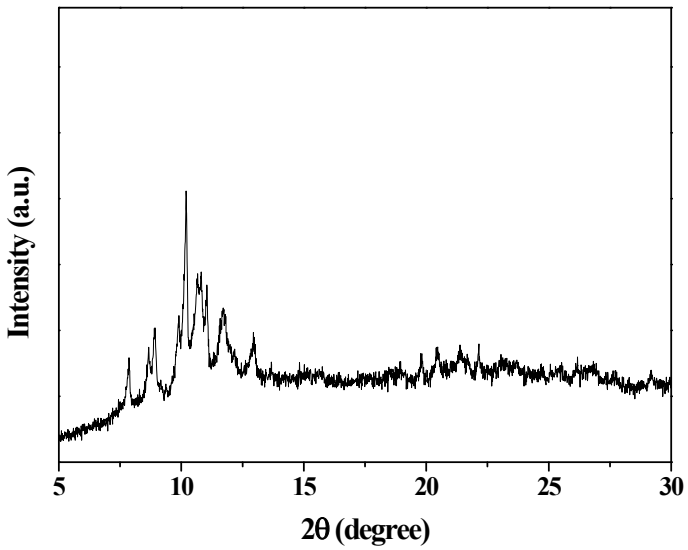

Fig. S1 XRD pattern of MIL-88(Fe) precursor.

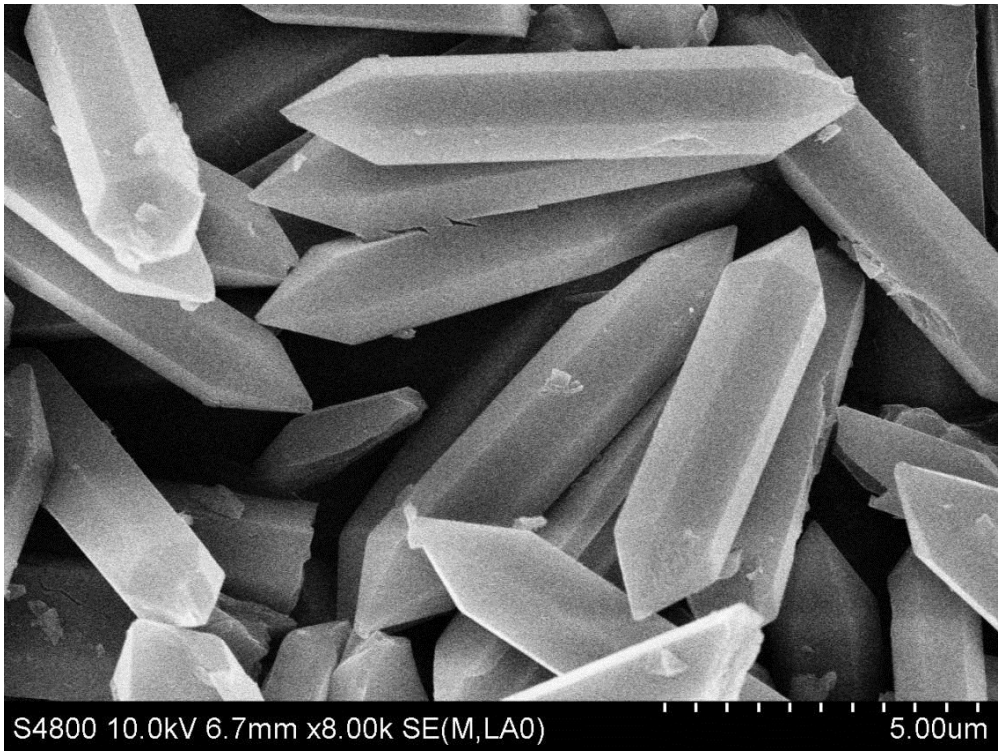

Fig. S2 FESEM image of MIL-88(Fe) precursor.

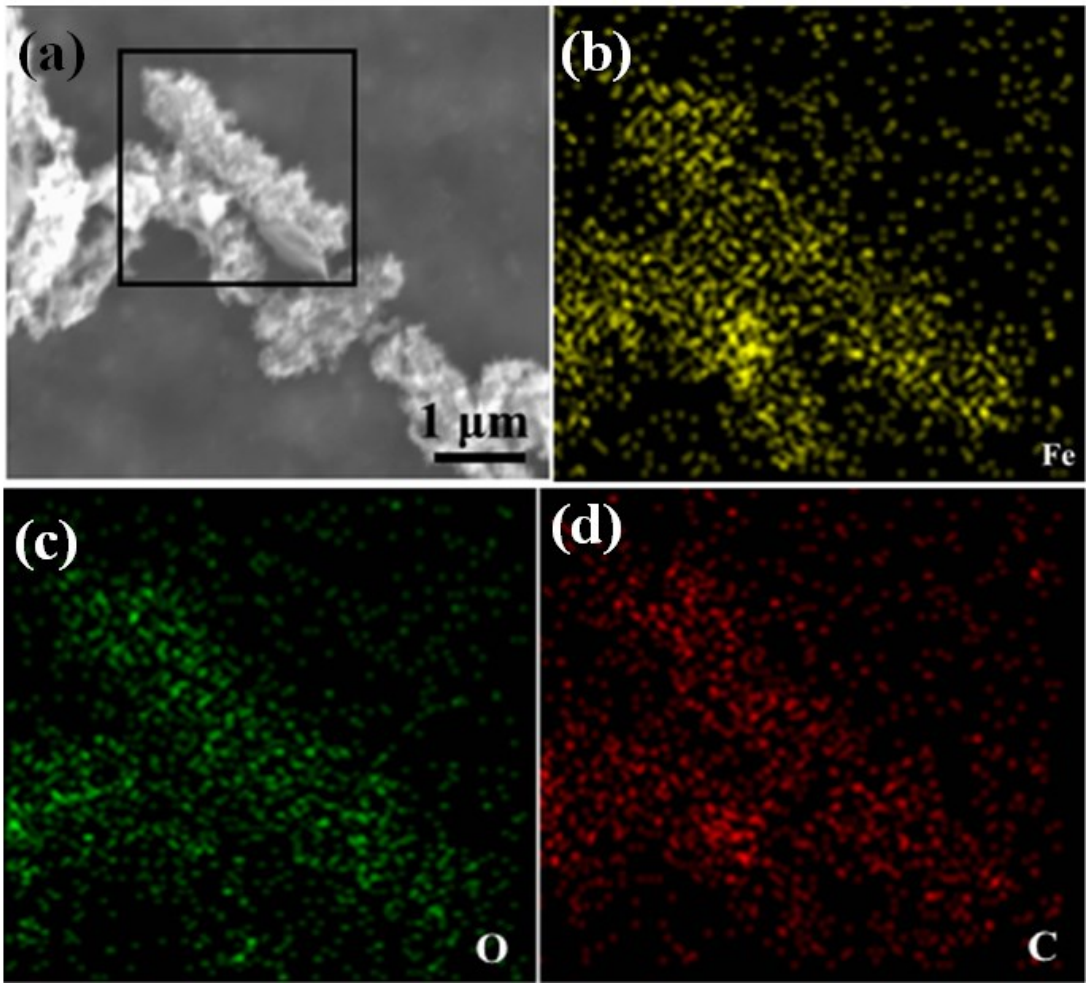

Fig. S3 EDS mapping of Fe_2O_3@C: (a) SEM image at selected area, EDS mapping for (b) Fe, (c) O and (d) C elements

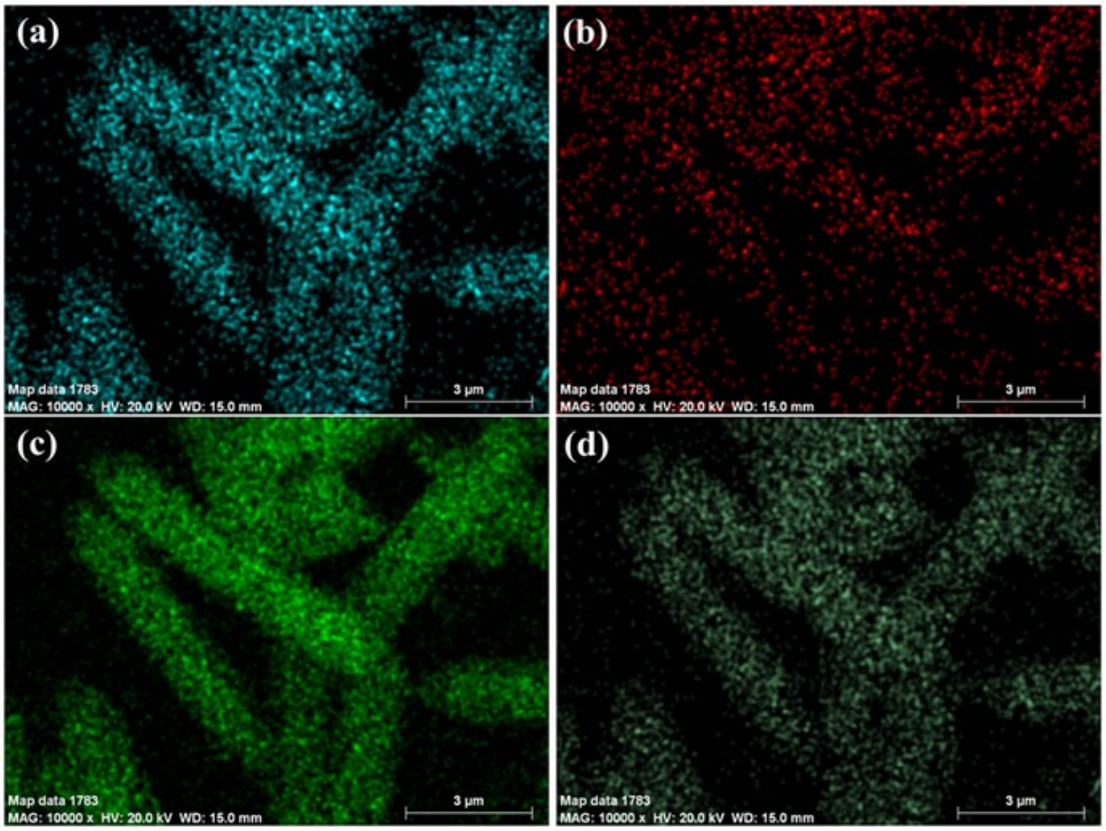

Fig. S4 EDS mappings of $Fe_2O_3/Fe_{1-x}S$@C for (a) Fe, (b) O, (c) S and (d) C elements.

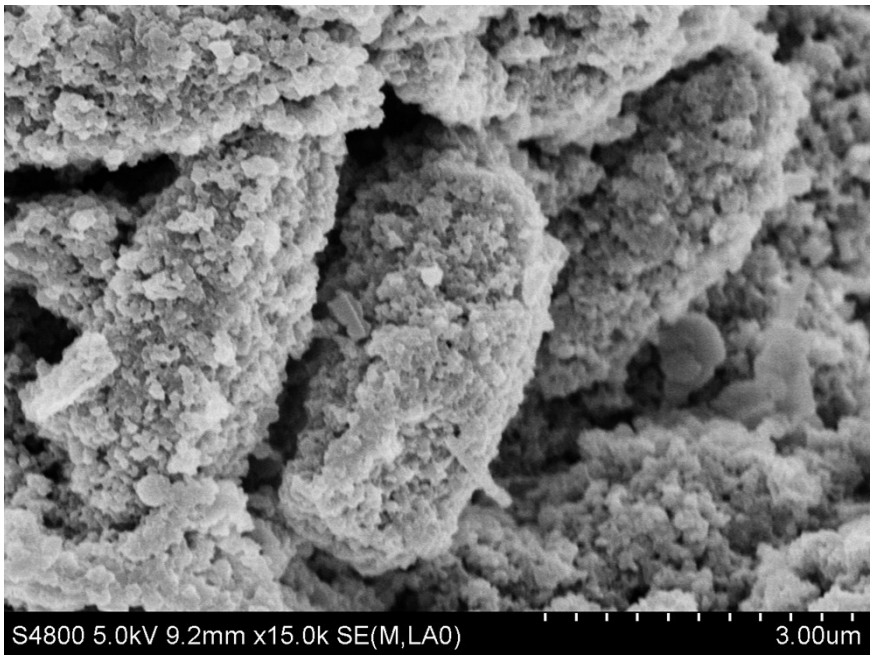

Fig. S5 FESEM image of $Fe_2O_3/Fe_{1-x}S$@C electrode after 100 cycles.

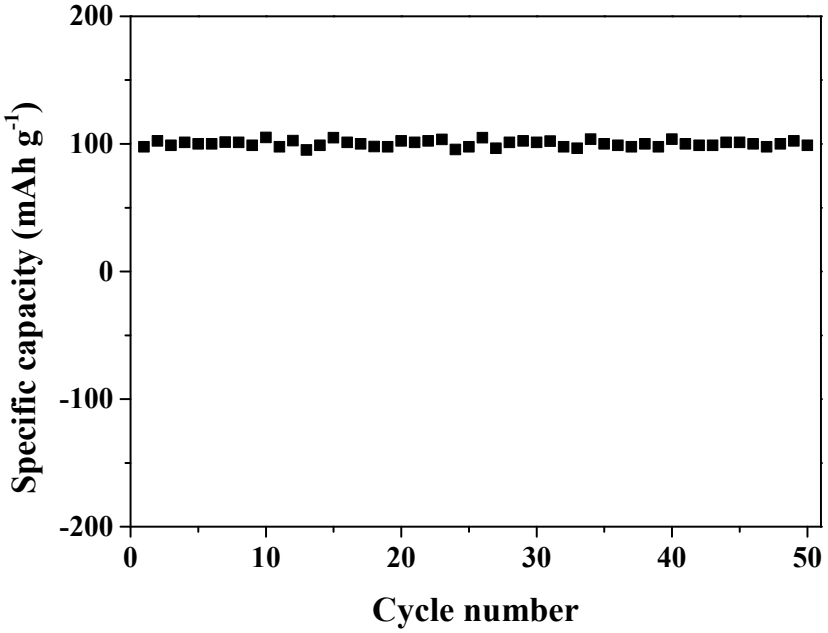

Fig. S6 The electrochemical performance of $Fe_2O_3/Fe_{1-x}S$@C at current density of 10 A g^{-1}.

Table S1 The element contents of Fe_2O_3@C and $Fe_2O_3/Fe_{1-x}S$@C.

Sample	Fe (wt. %)	C (wt. %)	O (wt. %)	S (wt. %)
Fe_2O_3@C	49.47	28.54	21.99	/
$Fe_2O_3/Fe_{1-x}S$@C	49.82	29.06	16.94	6.18

Table S2 Comparison of voltage range, specific capacity, rate capability and long-life cycling performance of $Fe_2O_3/Fe_{1-x}S$@C heterostructure in this work with other reported Fe_2O_3 and (or) FeS-based electrodes for LIBs.

Electrode materials	Voltage range	Current density (A g^{-1})	Specific capacity (mAh g^{-1})	References
$Fe_2O_3/Fe_{1-x}S$@C derived from MOFs	0.005-3 V	0.1, 0.2, 0.5, 1.0, 2.0, 5.0	1200, 1047, 875.6, 735.3, 546.1, 345	This work
Fe_2O_3@NCs	0.01-3 V	0.02, 0.04, 0.08, 0.2, 0.4, 0.8, 3.0	837.7, 791.5, 716.4, 661.8, 583.1, 514.4, 388.2	[1]
Fe_2O_3/carbon nanorods	0.01-3 V	0.2, 0.3, 0.5, 0.8	581, 534, 436, 352	[2]
Flower-like FeS/Fe_2O_3	0.05-3 V	0.1, 0.5, 2.0, 3.0, 4.0	906.7, 790, 460, 400, 390	[3]
Fe_2O_3/graphite	0.01-3 V	0.1, 0.2, 0.5, 1.0	965, 902, 789, 661	[4]
FeS nanofibers	0.001-3 V	0.2, 0.5, 1.0, 2.0, 3.0, 5.0	456, 437, 413, 394, 380, 353	[5]
Fe_2O_3@C and FeS@C nanofibers	0.005-3 V	1.0, 2.0, 4.0, 8.0, 16.0	949, 693, 556, 448, 316	[6]
$Fe_{1-x}S$	0.01-3 V	0.1, 0.2, 0.5, 1.0, 2.0, 5.0, 10	675, 671, 630, 608, 579, 539, 495	[7]
Fe_2O_3 nanoparticles	0.01-3 V	0.1, 0.2, 0.5,1, 2, 5	670, 550, 475, 423, 345, 220	[8]

References

[1] J. Zhu, L. Wei, J. Hu, C. Xue, Anchoring iron oxide nanoparticles on polypyrrole/rGO derived

nitrogen-doped carbon as lithium-ion battery anode, J. Alloy. Compd., 723 (2017) 729-735.

[2] Y. Sun, X. Liu, F. Huang, S. Li, Y. Shen, A. Xie, Spinach juice-derived porous Fe_2O_3/carbon nanorods as superior anodes for lithium-ion batteries, Mater. Res. Bull., 95 (2017) 321-327.

[3] J. Wang, H. He, Z. Wu, J. Liang, L. Han, H.L. Xin, X. Guo, Y. Zhu, D. Wang, Controllable construction of flower-like FeS/Fe_2O_3 composite for lithium storage, J. Power Sources, 392 (2018) 193-199.

[4] Y. Yan, H. Tang, F. Wu, Z. Xie, S. Xu, D. Qu, R. Wang, F. Wu, M. Pan, D. Qu, Facile synthesis of Fe2O3@graphite nanoparticle composite as the anode for Lithium ion batteries with high cyclic stability, Electrochim. Acta, 253 (2017) 104-113.

[5] J.S. Cho, J.-S. Park, Y.C. Kang, Porous FeS nanofibers with numerous nanovoids obtained by Kirkendall diffusion effect for use as anode materials for sodium-ion batteries, Nano Res., 10 (2017) 897-907.

[6] B. Wang, S. Zhang, G. Wang, H. Wang, J. Bai, The morphology and electrochemical properties of porous Fe_2O_3@C and FeS@C nanofibers as stable and high-capacity anodes for lithium and sodium storage, J. Colloid Interf. Sci., 557 (2019) 216-226.

[7] W. Nie, X. Liu, Q. Xiao, L. Li, G. Chen, D. Li, M. Zeng, S. Zhong, Hierarchical porous carbon anode materials derived from rice husks with high capacity and long cycling stability for sodium-ion batteries, ChemElectroChem, 7 (2020) 631-641.

[8] C. Duan, F. Zhu, C. Wang, X. Ke, G. Ren, Y. Meng, 3D Porous iron oxide/carbon with large surface area as advanced anode materials for lithium-ion batteries, Ionics, (2020), https://doi.org/10.1007/s11581-020-03574-w.